Accuracy of the Synchrophasor Estimator Returned by the Interpolated DFT Algorithm Under Off-Nominal Frequency and Harmonic Conditions

Daniel Belega
Department of Measurements and Optical Electronics
University Politehnica of Timisoara
Timisoara, Romania
daniel.belega@upt.ro

Dario Petri
Department of Electrical Engineering
University of Trento
Trento, Italy
dario.petri@unitn.it

***Abstract*—In this paper analytical expressions are derived for the synchrophasor amplitude and phase estimation errors achieved by the Interpolated Discrete Fourier Transform (IpDFT) algorithm when a steady-state harmonically distorted waveform at off-nominal frequency is weighted by a Maximum Sidelobe Decay (MSD) window. The derived expressions allow to separately analyze the contributions of the fundamental spectral image component, harmonics, and off-nominal frequency on the estimator Total Vector Error (*TVE*). Also, the related curves depicted in the plane of relative amplitude error and phase error allow to visually assess the overall accuracy of the IpDFT phasor estimator in the case of either pure sine-wave or harmonically distorted sine-waves. These curves are useful to analyze the robustness of the IpDFT algorithm to off-nominal frequency and harmonics.**

Keywords—Error analysis, interpolated DFT algorithm, parameter estimation, steady-state conditions, synchrophasor

I. Introduction

Proper protection and control of modern power grids requires accurate and real-time estimation of the synchrophasor amplitude and phase, frequency, and Rate-Of-Change Of Frequency (*ROCOF*) of the analyzed electrical waveforms. These parameters can be measured by the so-called Phasor Measurement Units (PMUs) [1], which exploit different time-domain or frequency-domain parameter estimation algorithms. Synchrophasor parameter estimates need to comply with the requirements of the IEEE Standard C37.118.1-2011 for Synchrophasor Measurements for Power Systems [2] and its Amendment [3]. These parameters are specified under the both steady-state and dynamic conditions, that is assuming either constant or time-varying waveform parameters. Two PMU performance classes have been conceived in that Standard, i.e., the *P-class* for protection purposes, and the *M-class* for measurement applications. In each performance class maximum allowed synchrophasor Total Vector Error (*TVE*), Frequency Error (*FE*), and *ROCOF* Error (*RFE*) are specified in different operating conditions representing situations often encountered in practice. However, the Standard does not consider harmonically distorted waveforms at off-nominal frequency, although this is a condition often encountered in practice.

The classical Discrete Fourier transform (DFT) algorithm is often adopted in PMUs since it can be easily implemented and provides accurate estimates when a steady-state waveform is acquired using quasi-coherent sampling, i.e., when the waveform frequency is very close to its nominal value of 50 Hz or 60 Hz. Unfortunately, in practice significant off-nominal frequency and/or dynamic conditions often occur so that the DFT algorithm can return poor estimates. Computer simulations showed that the Interpolated DFT (IpDFT) algorithm ensures accurate real-time synchrophasor amplitude and phase estimates under off-nominal frequency conditions even if the analyzed waveform is affected by harmonics [4]. Indeed that algorithm effectively compensates the so called picket-fence errors due to frequency discretization by determining the signal inter-bin frequency location through interpolation of the two highest DFT samples of the signal spectrum [5]-[8]. The IpDFT algorithm is often employed because it requires a small processing effort, especially when the Maximum Sidelobe Decay (MSD) cosine windows [9] are employed, since the related parameter estimators can be expressed using very simple analytical expressions [5]-[8]. In addition, these windows exhibit a very high spectrum sidelobe decay rate, thus ensuring high immunity to interference from disturbance tones such as the fundamental spectral image component, harmonics, and inter-harmonics [9]. The IpDFT algorithm has been recently employed also to obtain accurate waveform frequency and *ROCOF* estimates [10]-[12].

At the best of the authors' knowledge, when the IpDFT algorithm based on the MSD windows is applied to steady-state harmonically distorted sine-waves at off-nominal frequency, an analytical expression for the inter-bin frequency location error has been already published [13], but an expression for the synchrophasor amplitude and phase errors has not been derived yet. This is the aim of this paper. Moreover, the derived expressions allow to separately analyze the contributions of the fundamental spectral image component, harmonics, and off-nominal frequency on the estimator *TVE* and to compare them with the thresholds specified in the Standard [2]. Also, the curves achieved in the plane of relative amplitude error and phase error in the case of pure sine-wave and harmonically distorted sine-waves are determined and compared. This comparison is a very good indicator for the synchrophasor estimation accuracy achieved by means of the IpDFT algorithm.

II. Expressions for the Estimation Errors of Synchrophasor Amplitude, Phase, and TVE

Let's consider a discrete-time harmonically distorted sine-wave, expressed as:

978-1-5386-5375-3/18/$31.00 ©2018 IEEE

$$x(m) = \sum_{k=1}^{K} A_k \cos\left(2\pi k f\left(m+\frac{1}{2}\right)+\phi_k\right),$$

$$m = -\frac{M}{2}, -\frac{M}{2}+1, \ldots, \frac{M}{2}-1 \quad (1)$$

where A_k, $f_k = kf$, and ϕ_k are the amplitude, normalized frequency, and initial phase of the k-th harmonic, respectively ($k = 1$ corresponds to the fundamental component), K is the number of harmonics, and M is the even number of analyzed samples. The amplitude and phase of the fundamental component define the phasor p of the signal (1) by the expression $p \triangleq^{\text{def}} A_1 e^{j\phi_1}$ [1]. Since only steady-state conditions are considered in the following, all the parameters in (1) and the phasor p are assumed constant over time.

The normalized frequency f is defined as the ratio between the frequency f_{in} of the original continuous-time signal and the sampling frequency f_s. It can be expressed as:

$$f \triangleq^{\text{def}} \frac{f_{in}}{f_s} = \frac{\gamma}{M} = \frac{J+\delta}{M}, \quad (2)$$

in which $\gamma = J + \delta$ is the number of acquired signal cycles, where J is its integer part and δ ($-0.5 \le \delta < 0.5$) is the inter-bin frequency location. When f_{in} is equal to the nominal signal frequency f_0 (either 50 Hz or 60 Hz) it is assumed that exactly J signal cycles are acquired, i.e. that sampling is coherent and $\delta = 0$. Thus, the number of analyzed samples is $M = J \cdot f_s / f_0$. Conversely, when $f_{in} \neq f_0$ we have $\delta \neq 0$ and the related off-nominal frequency deviation is expressed by $\Delta f_{in} = f_{in} - f_0 = f_s \cdot \delta / M$.

To reduce the spectral leakage of the interfering tones (i.e. the fundamental spectral image component and harmonics) on the parameter estimated by the IpDFT algorithm, the signal (1) is weighted by a suitable window function $w(\cdot)$ and the analyzed signal is $x_w(m) = x(m) \cdot w(m)$. In the following, the H-term MSD window ($H \ge 2$) is considered, defined as:

$$w(m) \triangleq^{\text{def}} \sum_{h=0}^{H-1} a_h \cos\left(2\pi \frac{h}{M}\left(m+\frac{1}{2}\right)\right),$$

$$m = -\frac{M}{2}, -\frac{M}{2}+1, \ldots, \frac{M}{2}-1 \quad (3)$$

in which the window coefficients a_h are [8]: $a_0 = \frac{C_{2H-2}^{H-1}}{2^{2H-2}}, a_h = \frac{C_{2H-2}^{H-h-1}}{2^{2H-3}}$, $h = 1, 2, \ldots, H-1$, where $C_r^q = \frac{r!}{(r-q)!\, q!}$.

The Discrete-Time Fourier Transform (DTFT) of the windowed signal $x_w(m)$ is given by:

$$X_w(\lambda) \triangleq^{\text{def}} \sum_{m=-\frac{M}{2}}^{\frac{M}{2}-1} x_w(m) e^{-j\frac{2\pi}{M}\lambda\left(m+\frac{1}{2}\right)} = \sum_{k=1}^{K} \frac{A_k}{2}\left[W(\lambda - k\gamma)e^{j\phi} + W(\lambda + k\gamma)e^{-j\phi}\right], \ \lambda \in [0, M) \quad (4)$$

where $W(\cdot)$ is the DTFT of the window $w(\cdot)$. It can be shown that it is a real-valued even function (that is $W(-\lambda) = W(\lambda)$). Moreover, when $|\lambda| << M$ and $M >> 1$, we have [4]:

$$W(\lambda) = \frac{M \sin(\pi\lambda)}{2^{2H-2}\pi\lambda} \frac{(2H-2)!}{\prod_{h=1}^{H-1}(h^2-\lambda^2)}. \quad (5)$$

If $\hat{\delta}$ is the inter-bin frequency location estimator returned by the IpDFT algorithm, the related amplitude and phase estimators are given by [4]:

$$\hat{A}_1 \triangleq^{\text{def}} 2\frac{|X_w(J)|}{W(-\hat{\delta})} \quad (6)$$

and

$$\hat{\phi}_1 \triangleq^{\text{def}} angle\{X_w(J)\}, \quad (7)$$

For the signal (1), the IpDFT inter-bin frequency estimation error is given by [13]:

$$\Delta\delta \cong (H + (-1)^i\delta)(J+\delta) \times \left[\frac{(-1)^i 2}{2J+\delta+(-1)^{i+1}H}\frac{W(2J+\delta)}{W(\delta)}\cos(2\phi_1) + \sum_{k=2}^{K}\frac{(-1)^i(k-1)}{(k-1)J+k\delta+(-1)^i H}\frac{A_k}{A_1}\frac{W[(k-1)J+k\delta]}{W(\delta)}\cos(\phi_k - \phi_1)\right] \quad (8)$$

where $i = 0$ if $|X_w(J-1)| > |X_w(J+1)|$ and $i = 1$ if $|X_w(J-1)| < |X_w(J+1)|$.

The expressions for the corresponding relative amplitude error and phase estimation error are given in the following Propositions.

Proposition 1:

For the harmonically distorted signal (1), the relative amplitude estimation error of the IpDFT algorithm based on the H-term MSD window ($H \ge 2$) is given by:

$$e_a \triangleq \frac{\Delta A_1}{A_1} \triangleq^{\text{def}} \frac{\hat{A}_1 - A_1}{A_1} \cong \frac{W(2J+\delta)}{W(\delta)}\cos(2\phi_1) - \frac{W'(\delta)}{W(\delta)}\Delta\delta + \sum_{k=2}^{K}\frac{A_k}{A_1}\frac{W[(k-1)J+k\delta]}{W(\delta)}\cos(\phi_k - \phi_1), \quad (9)$$

where $W'(\delta)$ is the derivative of $W(\cdot)$ with respect to δ and $\Delta\delta = \hat{\delta} - \delta$ is the inter-bin frequency location estimation error.

Proposition 2:

For the harmonically distorted signal (1), the phase estimation error of the IpDFT algorithm based on the H-term MSD window ($H \ge 2$) is given by:

$$e_p \triangleq \Delta\phi_1 \triangleq^{\text{def}} \hat{\phi}_1 - \phi_1 \cong -\frac{W(2J+\delta)}{W(\delta)}\sin(2\phi_1) + \sum_{k=2}^{K}\frac{A_k}{A_1}\frac{W[(k-1)J+k\delta]}{W(\delta)}\sin(\phi_k - \phi_1). \quad (10)$$

The proofs of the Propositions 1 and 2 are given in the Appendixes A and B, respectively.

By substituting (8) into (9), after some algebra we obtain:

$$e_a \cong \rho_{ai}\cos(2\phi_1) + \sum_{k=2}^{K}\rho_{ah_k}\cos(\phi_k - \phi_1), \quad (11)$$

where $\rho_{ai} \triangleq \left[1 - \frac{(-1)^i 2(H+(-1)^i\delta)(J+\delta)}{2J+\delta+(-1)^{i+1}H}\frac{W'(\delta)}{W(\delta)}\right]\frac{W(2J+\delta)}{W(\delta)}$,

and $\rho_{ah_k} \triangleq \left[1 - \frac{(-1)^i(k-1)(H+(-1)^i\delta)(J+\delta)}{(k-1)J+k\delta+(-1)^i H}\frac{W'(\delta)}{W(\delta)}\right]\frac{A_k}{A_1}\frac{W[(k-1)J+k\delta]}{W(\delta)}$

Moreover, (10) can be written as:

$$e_p \cong -\rho_{pi}\sin(2\phi_1) + \sum_{k=2}^{K}\rho_{ph_k}\sin(\phi_k - \phi_1), \qquad (12)$$

where $\rho_{pi} \triangleq \frac{W(2J+\delta)}{W(\delta)}$ and $\rho_{ph_k} \triangleq \frac{A_k}{A_1}\frac{W[(k-1)J+k\delta]}{W(\delta)}$.

In (11) and (12) ρ_{ai} and ρ_{pi} represent the magnitudes of the contributions of the spectral image of the fundamental component on the amplitude and phase estimation errors, respectively, while ρ_{ah_k} and ρ_{ph_k} are the contributions due to the *k*-th harmonic.

From (8)-(12) it follows that:

i) the relative amplitude estimation error e_a depends upon the inter-bin frequency estimation error $\Delta\delta$, while the error e_p is almost independent of $\Delta\delta$;

ii) the contributions of the interfering tones on the errors e_a and e_p depend on cosine and sine functions of the argument $2\phi_1$ and $(\phi_k - \phi_1)$, respectively; hence, when one kind of error is maximum, the other is null;

iii) the errors e_a and e_p are null when coherent sampling occurs ($\delta = 0$);

iv) the magnitudes of the contributions of the interfering tones on the errors e_a and e_p decrease as the number of acquired signal cycles γ and k increase;

v) the most relevant contributions to the errors e_a and e_p are due to the spectral image of the fundamental component and the 2nd harmonic.

Fig. 1 shows the magnitudes of the contributions ρ_{ai}, ρ_{ah_2}, ρ_{ah_3}, ρ_{ah_4}, ρ_{pi}, ρ_{ph_2}, ρ_{ph_3}, and ρ_{ph_4} as a function of the frequency deviation Δf_{in} when J = 3 or 4 nominal cycles are observed and the amplitudes of the fundamental component and the harmonics are 1 p.u. and 0.1 p.u., respectively, as suggested for the worst-case operating conditions in the *M-class* of performance by the Standard for synchrophasor measurements [2].

As for the amplitude error, for both J = 3 and 4 cycles, Fig. 1 shows that the contribution of the 2nd harmonic is higher than the one related to the fundamental spectral image when $\Delta f_{in} < 0$ Hz (i.e. $\delta < 0$). When $0 < \Delta f_{in} < 1$ Hz the two contributions are almost equal, while the spectral image of the fundamental component is less attenuated when $\Delta f_{in} > 1$ Hz. In the case of phase error the contribution of the 2nd harmonic is higher than the one related to the fundamental spectral image component when Δf_{in} is less than about 3 Hz and it is much higher when $\Delta f_{in} < 0$ Hz. For the remaining values of Δf_{in} we have $\rho_{pi} > \rho_{ph_2}$. From Fig. 1 it also follows that the contributions to errors e_a and e_p, due to the 3rd and 4th harmonics are much smaller than those related to the 2nd harmonic or the fundamental spectral image component. Finally, it is worth observing that both errors e_a and e_p are almost null when Δf_{in} = 0 Hz (i.e. coherent sampling occurs).

The behavior of the curve $f(e_a, e_p)$ in the (e_a, e_p) plane provides a useful indicator of the estimators accuracies [10], [14]. When the harmonic contribution is negligible, from (11) and (12) we obtain:

$$\frac{e_a^2}{\rho_{ai}^2} + \frac{e_p^2}{\rho_{pi}^2} - 1 = 0, \qquad (13)$$

which represents the equation of an ellipse with semi-axes ρ_{ai} and ρ_{pi}. Conversely, when harmonics are not negligible, by varying the argument $(\phi_k - \phi_1)$ of the cosine and sine functions in (11) and (12), the points (e_a, e_p) cover a limited surface, as will be seen in the next Section.

As for the *TVE*, for small values of the errors e_a and e_p, we have [15]:

$$TVE \overset{\text{def}}{=} \sqrt{\frac{(\hat{X}_r - X_r)^2 + (\hat{X}_i - X_i)^2}{X_r^2 + X_i^2}} \cong \sqrt{e_a^2 + e_p^2}, \qquad (14)$$

where X_r and X_i are the theoretical real and imaginary parts of the phasor p, while $\hat{X}_r$ and $\hat{X}_i$ are their estimates.

III. Computer Simulations

In this Section the accuracies of the expressions derived in Section II are verified through computer simulations. Also, the accuracies of the IpDFT estimators are graphically analyzed in the (e_a, e_p) plane.

As in the previous Section, the amplitudes of the fundamental component and the harmonics (when present) are 1 p.u. and 0.1 p.u., respectively. The nominal frequency is f_0 = 50 Hz and the sampling rate is f_s = 6 kHz, resulting in 120 samples/nominal cycle. The frequency deviation Δf_{in} is in the range [-5, 5] Hz, as suggested in the Standard [2]. J = 3 or 4 nominal cycles are considered since (11) and (12) exhibit low accuracy when $\gamma \leq 2$ cycles due to the adopted approximations (see Appendices A and B). For each value of the frequency deviation Δf_{in}, 1000 runs of $M = 120 \cdot J$ samples each are considered in which the initial phases of all signal tones are varied at random. The two-term MSD window, also known as the Hann window [9], is adopted.

Fig. 2 shows the estimated magnitudes of the phasor *TVE* as a function of the frequency deviation Δf_{in} returned by simulations and (11) or (12) when the signal (1) is affected by a 2nd harmonic (Fig. 2(a)) or a 3rd harmonic (Fig. 2(b)).

As we can see, the simulation and theoretical results are very close to each other. Moreover, Fig. 2 confirms that the *TVE* decreases as J or the harmonic order increase. In addition, the obtained *TVE* values are below the 1% threshold defined in the Standard for the *M-class* of performance in both considered situations.

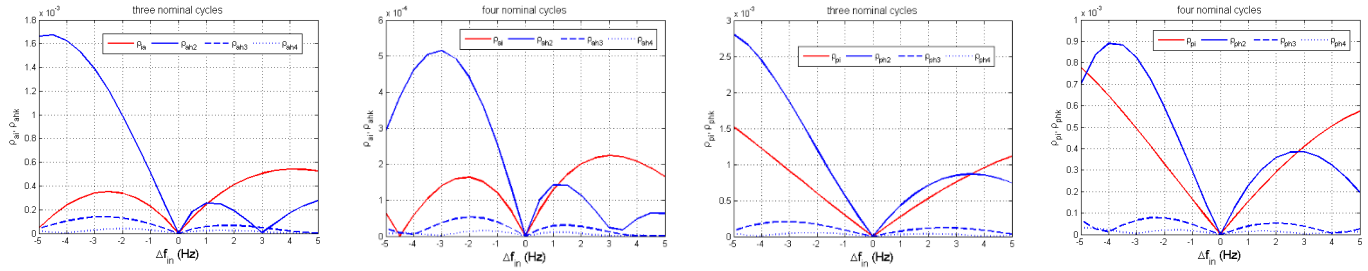

(a) (b) (c) (d)

Fig. 1. Magnitudes of the contributions of the spectral image of the fundamental component, 2nd, 3rd, and 4th harmonics on the relative amplitude error e_a (ρ_{ai}, ρ_{ah_2}, ρ_{ah_3}, and ρ_{ah_4}) (a), (b) and the phase error e_p (ρ_{pi}, ρ_{ph_2}, ρ_{ph_3}, and ρ_{ph_4}) (c), (d) versus the frequency deviation Δf_{in} (in Hz) when $J = 3$ or 4 nominal cycles.

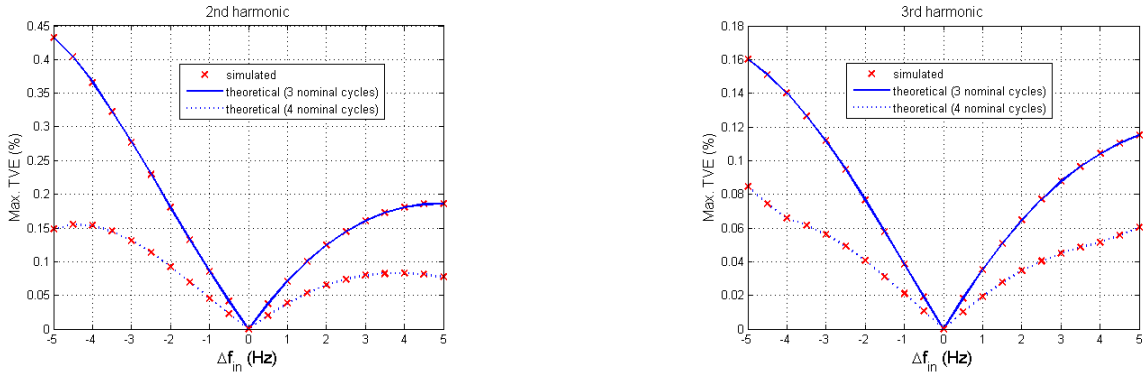

(a) (b)

Fig. 2. Magnitudes of the *TVE* returned by the IpDFT algorithm based on the Hann window and (14) versus the frequency deviation Δf_{in} (in Hz) for signal (1) affected by a 2nd harmonic (a) or a 3rd harmonic (b). $J = 3$ or 4 nominal cycles and 1000 runs of $M = 120 \cdot J$ samples each are considered. Fundamental and harmonic phases chosen at random in the range [0, 2π) rad.

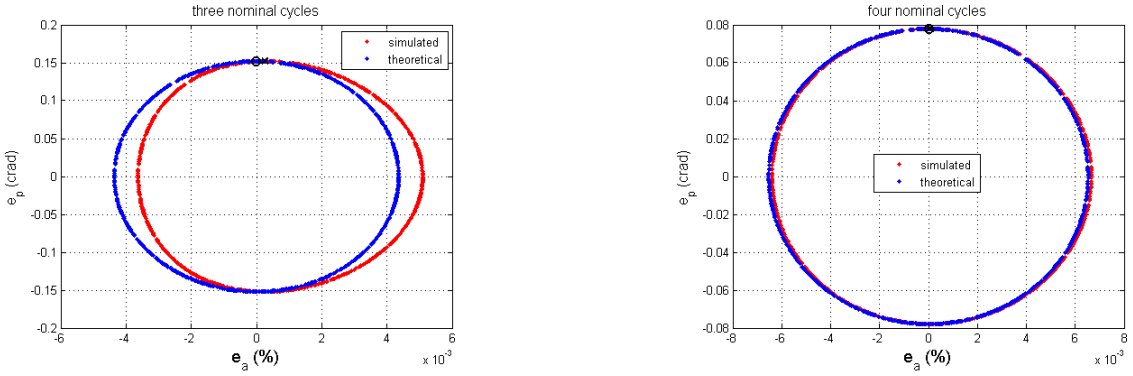

(a) (b)

Fig. 3. Curves $f(e_a, e_p)$ obtained by means of (13) and simultaions when applying the IpDFT algorithm based on the Hann window to a pure sine-wave. $J = 3$ (a) or 4 (b) nominal cycles and off-nominal frequency deviation $\Delta f_{in} = -5$ Hz. The points corresponding to the maximum *TVE* values obtained through simulations ('x') and theory ('o') are shown. 1000 runs of $M = 120 \cdot J$ samples each with the fundamental phase chosen at random in the range [0, 2π) rad.

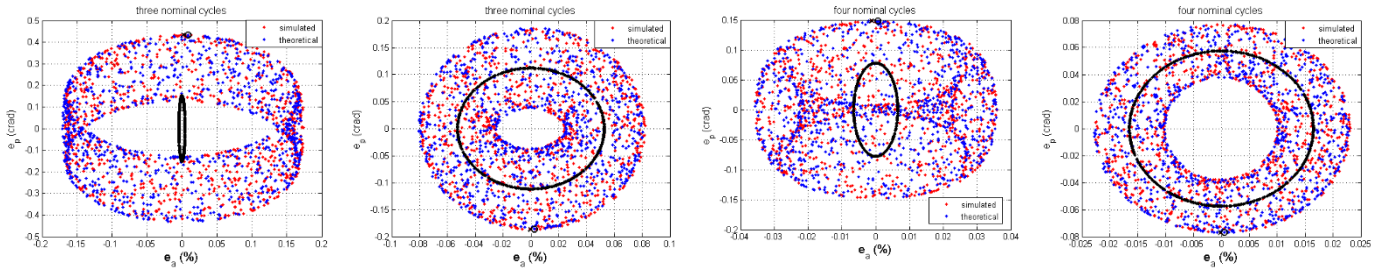

(a) (b) (c) (d)

Fig. 4. Curves $f(e_a, e_p)$ obtained by means of (13) and simulations when applying the IpDFT algorithm based on the Hann window to a sine-wave affected by a 2nd harmonic with amplitude 10% of the fundamental. $J = 3$ (a), (b) or 4 (c), (d) nominal cycles and off-nominal frequency deviation $\Delta f_{in} = -5$ Hz (a), (c) or $\Delta f_{in} = 5$ Hz (b), (d). The curves $f(e_a, e_p)$ returned by (13) when the effect of harmonic is neglected are shown by using a solid line. The points corresponding to the maximum *TVE* values obtained through simulations ('x') and theory ('o') are also shown. 1000 runs of $M = 120 \cdot J$ samples each with the fundamental phase chosen at random in the range $[0, 2\pi)$ rad.

Fig. 3 shows the curves $f(e_a, e_p)$ obtained by simulations and (11), (12), (13) in the case of a pure sine-wave with $\Delta f_{in} = -5$ Hz, which corresponds to the worst-case condition considered in the Standard [2]. The points corresponding to the maximum *TVE* values obtained through simulations and theory are also reported in Fig. 3.

From Fig. 3 it is evident that the ellipses returned by simulations and theory slightly differ to each other when $J = 3$ nominal cycles, while they almost coincide when $J = 4$ nominal cycles. Also, the points obtained by simulations and (13) that correspond to the maximum *TVE* value are very close to each other in both cases and they are almost due to the phase error e_p, while the corresponding relative amplitude error e_a is negligible.

Fig. 4 shows the points (e_a, e_p) obtained by simulations and (11), (12), (13) when the signal (1) contains a 2nd harmonic and the off-nominal frequency deviation is $\Delta f_{in} = -5$ Hz or 5 Hz. Also, the curves $f(e_a, e_p)$ returned by (13) when the effect of harmonic is neglected are shown.

As it can be seen, the obtained points belong to a surface that enclose the curve $f(e_a, e_p)$ related to the fundamental component. That dispersion is due to the cosine and sine terms with argument $(\phi_k - \phi_1)$ in (11) and (12) and it increases as the contribution of the 2nd harmonic increases. Thus, the highest dispersion corresponds to $J = 3$ nominal cycles and $\Delta f_{in} = -5$ Hz, while the smallest one is obtained when $J = 4$ nominal cycles and $\Delta f_{in} = 5$ Hz. In all the considered situations the points corresponding to the maximum *TVE* values obtained through either simulations or theory are very close to each other and they are related to a negligible relative amplitude error e_a. It is worth noticing that, since the contribution of higher order harmonics is negligible as compared with the 2nd order one (see Fig. 1), the graphs reported in Fig. 4 provide useful and quite accurate information about the overall rejection capabilities of interfering tones of the IpDFT amplitude and phase estimators.

IV. Conclusions

This paper has been aimed at the derivation of analytical expressions for the synchrophasor amplitude and phase estimation errors achieved when the IpDFT algorithm based on the MSD windows is applied to a harmonically distorted sine-wave with off-nominal frequency. The derived expressions have been verified through computer simulations. Moreover, curves and surfaces in the plane of relative amplitude error and phase error obtained in the case of either pure or harmonically distorted sine-waves allow to visually assess the overall accuracy achievable by the IpDFT algorithm. In particular, the contributions of both off-nominal frequency and harmonics on the estimation accuracy have been examined. It has been shown that, thanks to windowing, the contributions of the third and higher order harmonics can be neglected when at least 3 or 4 signal cycles are observed.

Appendix A
Derivation of the expression for the relative amplitude estimation error e_a

Assuming that at least $H + 1$ nominal cycles of the signal (1) are observed, the terms that represent in (4) the spectral image of harmonics are very small as compared with the other terms and can be neglected [13]. Thus, after some calculations, we achieve:

$$|X_w(J)| \cong \frac{A_1}{2} W(\delta) + \frac{A_1}{2} W(2J + \delta) \cos(2\phi_1) + \sum_{k=2}^{K} \frac{A_k}{2} W[(k-1)J + k\delta] \cos(\phi_k - \phi_1). \quad (A.1)$$

Since the inter-bin frequency location estimation error $\Delta\delta = \hat{\delta} - \delta$ is small, $W(\hat{\delta})$ can be expressed by truncating its Taylor's series about δ to the first order term:

$$W(\hat{\delta}) \cong W(\delta) + W'(\delta)\Delta\delta, \quad (A.2)$$

where $W'(\delta)$ is the derivative of $W(\cdot)$ with respect to δ.

By substituting (A.1) and (A.2) into (6) we obtain:

$$\hat{A}_1 \cong [A_1 W(\delta) + A_1 W(2J + \delta) \cos(2\phi_1) + \sum_{k=2}^{K} A_k W[(k-1)J + k\delta] \cos(\phi_k - \phi_1)] \times \left[W(\delta)\left(1 + \frac{W'(\delta)}{W(\delta)}\Delta\delta\right)\right]^{-1}. \quad (A.3)$$

Since $\left|\frac{W'(\delta)}{W(\delta)}\Delta\delta\right| \ll 1$, the approximation $(1 + x)^{-1} \cong 1 - x$, with $|x| << 1$, can be applied in (A.3). Moreover the terms containing the

products $W(2J+\delta)\cdot W'(\delta)$ and $W[(k-1)J+k\delta]\cdot W'(\delta)$, $k = 2, 3,\ldots, K$ are very small as compared with the other terms and can be neglected. Consequently, after some algebra we obtain:

$$\hat{A}_1 \cong A_1 + A_1\frac{W(2J+\delta)}{W(\delta)}\cos(2\phi_1) - A_1\frac{W'(\delta)}{W(\delta)}\Delta\delta + \sum_{k=2}^{K} A_k\frac{W[(k-1)J+k\delta]}{W(\delta)}\cos(\phi_k-\phi_1). \quad (A.4)$$

Finally, expression (9) can be easily achieved from (A.4).

APPENDIX B
Derivation of the expression for the relative amplitude estimation error e_p

Assuming that at least $H + 1$ nominal cycles of the signal (1) are observed, the terms that represent in (4) the spectral image of harmonics can be neglected [13]. Thus, after some algebra we obtain:

$$\hat{\phi}_1 = angle\{X_w(J)\} \cong \tan^{-1}\left(\frac{1-\frac{W(2J+\delta)}{W(\delta)}+\sum_{k=2}^{K}\frac{A_k}{A_1}\frac{W[(k-1)J+k\delta]}{W(\delta)}\frac{\sin(\phi_k)}{\sin(\phi_1)}}{1+\frac{W(2J+\delta)}{W(\delta)}+\sum_{k=2}^{K}\frac{A_k}{A_1}\frac{W[(k-1)J+k\delta]}{W(\delta)}\frac{\cos(\phi_k)}{\cos(\phi_1)}}\tan(\phi_1)\right). \quad (B.1)$$

Since $\left|\frac{W(2J+\delta)}{W(\delta)}+\sum_{k=2}^{K}\frac{A_k}{A_1}W[(k-1)J+k\delta]\frac{\cos(\phi_k)}{\cos(\phi_1)}\right| \ll 1$, the approximation $(1 + x)^{-1} \cong 1- x$, where $|x| << 1$ can be applied in (B.1). Moreover, the terms containing the factors $W^2(2J+\delta)$, $W(2J+\delta)\cdot W[(k-1)J+k\delta]$ and $W[(l-1)J+l\delta]\cdot W[(k-1)J+k\delta]$, $k, l = 2, 3,\ldots,K$ are very small as compared with the other terms and can be neglected. Thus, after some calculations we obtain:

$$\hat{\phi}_1 \cong \tan^{-1}\left[\tan(\phi_1) - 2\frac{W(2J+\delta)}{W(\delta)}\tan(\phi_1) + \sum_{k=2}^{K}\frac{A_k}{A_1}\frac{W[(k-1)J+k\delta]}{W(\delta)}\sin(\phi_k-\phi_1)\right]. \quad (B.2)$$

Since $W(\delta) >> W(2J + \delta)$ and $W(\delta) >> W[(k - 1)J + k\delta]$, the $\tan^{-1}(\cdot)$ function can be expressed by truncating its Taylor's series about $\tan(\phi_1)$ to the first order term. Thus, after some algebra, (B.2) becomes:

$$\hat{\phi}_1 \cong \phi_1 - \frac{W(2J+\delta)}{W(\delta)}\sin(2\phi_1) + \sum_{k=2}^{K}\frac{A_k}{A_1}\frac{W[(k-1)J+k\delta]}{W(\delta)}\sin(\phi_k-\phi_1). \quad (B.3)$$

Finally, expression (10) can be easily achieved from (B.3).

REFERENCES

[1] A.G. Phadke and J.S. Thorp, Synchronized Phasor Measurements and Their Applications, New York: Springer-Science, 2008.

[2] IEEE Standard C37.118.1 for Synchrophasor Measurements for Power Systems, Dec. 2011.

[3] Amendment 1: Modification of Selected Performance Requirements, to IEEE Standard C37.118.1-2011 for Synchrophasor Measurements for Power Systems, IEEE Standard C37.118.1a-2014.

[4] D. Belega and D. Petri, "Accuracy analysis of the multicycle synchrophasor estimator provided by the interpolated DFT algorithm," IEEE Trans. Instrum. Meas., vol. 62, no. 5, pp. 942-953, May 2013.

[5] D.C. Rife and G.A. Vincent, "Use of the discrete Fourier transform in the measurement of frequencies and levels of tones," Bell Syst. Tech. J., vol. 49, pp. 197-228, 1970.

[6] T. Grandke, "Interpolation algorithms for discrete Fourier transforms of weighted signals," IEEE Trans. Instrum. Meas., vol. IM-32, no. 2, pp. 350 – 355, Jun. 1983.

[7] C. Offelli and D. Petri, "The influence of windowing on the accuracy of multifrequency signal parameter estimation," IEEE Trans. Instrum. Meas., vol. 41, no. 2, pp. 256-261, Apr.1992.

[8] D. Belega and D. Dallet, "Multifrequency signal analysis by interpolated DFT method with maximum sidelobe decay windows," Measurement, vol. 42, no. 3, pp. 420-426, Apr. 2009.

[9] A.H. Nuttall, "Some windows with very good sidelobe behavior," IEEE Trans. Acoust., Speech, Signal Processing, vol. ASSP-29, no.1, pp 84–91, Feb. 1981.

[10] D. Belega, D. Fontanelli, and D. Petri, "Dynamic Phasor and Frequency Measurements by an Improved Taylor Weighted Least Squares Algorithm," IEEE Trans. Instrum. Meas., vol. 64, no. 8, pp. 2165-2178, Aug. 2015.

[11] P. Romano and M. Paolone, "Enhanced interpolated-DFT for synchrophasor estimation in FPGAs: theory, implementation, and validation of a PMU prototype," IEEE Trans. Instrum. Meas., vol. 63, no. 12, pp. 2824-2836, Dec. 2014.

[12] A. Derviškadić, P. Romano, and M. Paolone, "Iterative-interpolated DFT for synchrophasor estimation: a single algorithm for P- and M-cass compliant PMUs," IEEE Trans. Instrum. Meas., vol. 67, no. 3, pp. 547-558, Mar. 2018.

[13] D. Belega, D. Petri, and D. Dallet, "Impact of harmonics on the interpolated DFT frequency estimator," Mech. Syst. Signal Process., vols. 66-67, pp. 349-360, Jan. 2016.

[14] G. Barchi, D. Macii, D. Belega, and D. Petri, "Performance of Synchrophasor Estimators in Transient Conditions: A Comparative Analysis," IEEE Trans. Instrum. Meas., vol. 62, no. 9, pp. 2410-2418, Sep. 2013.

[15] P. Castello, M. Lixia, C. Muscas, and P.A. Pegoraro, "Impact of the model on the accuracy of synchrophasor measurement," IEEE Trans. Instrum. Meas., vol. 61, no. 8, pp. 2179-2188, Aug. 2012.